Surface properties of chitin-glucan nanopapers from *Agaricus bisporus*

Wan Mohd Fazli Wan Nawawi[a,b,c], Koon-Yang Lee[d], Eero Kontturi[e], Alexander Bismarck[a,f], Andreas Mautner[a,*]

[a] *Institute of Materials Chemistry & Research, Polymer & Composite Engineering (PaCE) Group, University of Vienna, Währingerstr. 42, A-1090 Vienna, Austria*

[b] *Polymer & Composite Engineering (PaCE) Group, Department of Chemical Engineering, Imperial College London, SW7 2AZ London, United Kingdom*

[c] *Department of Biotechnology Engineering, International Islamic University Malaysia, P.O. Box 10, 50728 Kuala Lumpur, Malaysia*

[d] *Department of Aeronautics, Imperial College London, South Kensington Campus, London, SW7 2AZ, UK*

[e] *Department of Bioproducts and Biosystems (BIO2), School of Chemical Engineering, Aalto University, PO Box 16300, FI-00076 Aalto, Finland*

[f] *Department of Mechanical Engineering, Faculty of Engineering and the Built Environment, University of Johannesburg, South Africa*

* Corresponding author: e-mail: andreas.mautner@univie.ac.at

Abstract

The structural component of fungal cell walls comprises of chitin covalently bonded to glucan; this constitutes a native composite material (chitin-glucan, CG) combining the strength of chitin and the toughness of glucan. It has a native nano-fibrous structure in contrast to nanocellulose, for which further nanofibrillation is required. From fungal chitin nanofibrils (FChNFs) nanopapers can be manufactured. FChNF nanopapers are potentially applicable in packaging films, composites or membranes for water treatment due to their distinct surface properties inherited from the composition of chitin and glucan. Here, chitin-glucan nanofibrils were extracted from common mushroom (*Agaricus bisporus*) cell walls utilizing a mild isolation procedure to preserve the native quality of the chitin-glucan complex. These extracts were readily disintegrated into nanofibre dimensions by a low-energy mechanical blending, thus making the extracts dispersion directly suitable for nanopaper preparation using a simple vacuum filtration process. Chitin-glucan nanopaper morphology,

mechanical, chemical and surface properties were studied and compared to chitin nanopapers of crustacean (*Cancer pagurus*) origin. It was found that fungal extract nanopapers had distinct physico-chemical surface properties, being more hydrophobic than crustacean chitin.

Keywords: *agaricus bisporus*; nanopaper; surface properties.

1. Introduction

Nano-sized fibrillar structures, such as polymer nanofibres or carbon nanotubes are currently a hot-topic in material science because of their high strength and modulus [1]. Thus, also natural nano-fibrils are an appealing approach to integrate the advantages of nano-scale fibres with sustainable raw materials. The combination of nanosized fibres extracted from renewable raw materials thus constitutes an important direction in the chase for novel sustainable materials solutions [2, 3].

Recently, cellulose has attracted renewed interest in this field, mostly because it can be nanofibrillated [4]. A large variety of composites [2, 5] but also membrane applications [6-8] have been developed from this class of material. In this regard, using nanocellulose in a macroscopic sheet, i.e. nanopaper, has shown particularly great potential [9-13]. Next to cellulose, chitin is the second most abundant renewable polymer. Even though Braconnot's isolation of chitin [14, 15] preceded Payen's discovery of cellulose [16] by almost 30 years, research and applications of chitin are lagging behind those of cellulose. Similar to cellulose and its function in green plants, the primary biological function of chitin is to provide the structural scaffold supporting the exoskeleton of crustacean and insects or the fungal cell wall [17]. This function is fulfilled differently in these forms of life due to their different physiochemical properties. In shellfish, chitin is normally associated with sclerotized proteins and minerals, while in fungi, depending on the species, chitin is combined with other polysaccharides such as glucan, mannan, or chitosan [18]. So far, most reports deal with the preparation of chitin derived from animal sources and (nano)papers or films prepared therefrom [19-34], although, the potential of fungal chitin was recognized quite early on [35].

In fungi, chitin and glucan are covalently linked, which was shown in several studies. Unlike animal-derived chitin, in which the residual compounds such as proteins or other polysaccharides, are

present in minor fractions, fungal chitin contains significant proportions of glucan, often even higher than that of chitin itself [36-43]. This is, however, not considered a drawback per se but actually constitutes a big advantage of fungal chitin as it provides different physico-chemical and surface properties as compared to crustacean chitin. Fungal chitin is also free from the crustacean allergenic protein, tropomyosin [44], which further extends its potential usability. This was demonstrated by KitoZyme [45] having extracted a chitin-glucan complex from the black mold *Aspergillus niger*, which is now marketed as food supplement [46]. Moreover, fungal chitin nanofibrils (FChNF) carry already their matrix, i.e. covalently attached glucan, which improves film forming properties. In such films or FChNF nanopapers, the chitin nanofibrils provide strength and stiffness while glucan increases flexibility and toughness but also determines its surface properties. Further differences between animal and fungal chitin are summarized in [47].

Whereas chitin nanomaterials derived from animal sources have been proposed as a renewable nano-reinforcement for composite production, the uncertainty and inconsistency of shellfish availability, which is subject to seasonal and regional supply fluctuations intensifies the need of considering fungal chitin as a viable alternative to animal-based chitin. Furthermore, chitin in fungi is already present in the form of nanofibrils, which can be extracted from fungal cell biomass by mild alkaline extraction followed by low-energy blending, making it not only a potential alternative to animal chitin but also to nanocellulose [48, 49]. Therefore, FChNF could offer a valuable source to new chitin based materials, applicable in packaging materials, e.g. mycelium composites [49], composites but also for water treatment.

In this study, chitin-glucan (CG) was extracted from common mushroom *Agaricus bisporus* (AB) and nanopapers were prepared. CG was isolated from AB cell walls from different parts of the fungi, i.e. stalk, cap, and whole fruiting body, utilizing a mild procedure. The chemical composition and physical properties of the extract were analyzed and the morphology of the nanofibrils studied. Nanopapers of varying grammage and thickness were prepared by vacuum filtration of homogeneous FChNF dispersions and their morphology and mechanical, chemical and surface properties evaluated

in dependence of their thickness and compared to crustacean (*Cancer pagurus*) chitin nanofibers (ChNF).

2. Materials & methods

2.1. Materials

Common white button mushrooms, *A. bisporus*, were purchased from a local store (London, UK). As reference material, untreated carapaces of brown edible crab, *Cancer pagurus*, were purchased from C-Quest Ltd. (Dorset, UK). Chitin flakes from shrimp shells served as further reference and were purchased from Sigma-Aldrich (C9213, practical grade). Prior to use they were finely ground in a ball mill. Hydrochloric acid (Sigma-Aldrich, 37% w/w), sodium hydroxide (Sigma Aldrich, pellets) and sulfuric acid (Merck, 72% w/w) were used for chitin extraction and sugar hydrolysis. Sugar Recovery Standards (SRS) for carbohydrate analysis were prepared from D-(+)-glucose (BDH Prolabo), D-(+)-xylose (Merck), D-(+)-galactose (Merck), D-(+)-arabinose (Chalbiochem), D-(+)-rhamnose (BDH Prolabo), D-(+)-mannose (Merck), and D-(+)-glucosamine hydrochloride (Sigma-Aldrich). n-Hexane, n-heptane, octane, nonane, decane, dichloromethane, ethyl acetate, acetonitrile, and acetone for specific surface area and surface energy analysis by inverse gas chromatography (iGC) were HPLC grade purchased from Sigma-Aldrich. Test liquids used for wicking tests were analytical grade benzylalcohol (Sigma-Aldrich, purity ≥ 99%), formamide (Sigma-Aldrich, purity ≥ 99.5%), decalin (Riedel-de Haën, purity ≥ 98%), and ethyleneglycol (Arcos Organic, purity ≥ 99.9%). Ultrapure water (CENTRA-R 200 or PURELAB Classic, 0.055 µS cm^{-1} conductivity, <10 ppb inorganic impurities) was used for all experiments.

2.2. Extraction of chitin

2.2.1. Extraction of FChNF from fungi

Prior to FChNF extraction, 500 g mushrooms with an average cap diameter of 50 to 70 mm, were rinsed with distilled water to remove any dirt and soil, followed by 5 min initial blending in a kitchen blender (Breville VBL065 Pro 800W, Oldham, UK). Afterwards, this mushroom slurry was diluted

to 1.5 L and heated to 85 °C under stirring for 30 min to remove any water soluble components. The suspension was then centrifuged at 7000 rpm for 15 min (ThermoScientific, Sorvall Legend RT+) to remove excess water together with the soluble components. The gel obtained after centrifugation was soaked in alkaline solution (1 M NaOH, total volume 1.5 L) and heated to 65 °C under stirring for 3 h to deproteinate and remove lipids as well as alkali-soluble glucan [50, 51]. Thereafter, the slurry was neutralized by successively re-centrifuging and exchanging excess water with fresh one. The neutral gel was re-suspended in water (0.8% w/v) and blended for another 1 min. This suspension was stored at 4 °C prior use [48]. Apart from using never dried suspension, parts of the extracts were also freeze-dried (ThermoScientific, Heto PowerDry LL1500 Freeze Dryer). Freeze-dried samples were used for elemental and sugar analysis, density and surface area determination.

2.2.2. ChNF extraction from crab shells

ChNF from crabs shells (*C. pagurus*) with an average width of approximately 120 to 160 mm were oven dried at 60 °C, crushed into smaller pieces, and ground for 5 min in a ball mill giving an average particle size of 150–300 μm. A similar extraction procedure as described in Section 2.2.1 was utilized except that an additional demineralization step had to be performed between hot water extraction and deproteination: 1 M HCl was added to the gel after centrifugation (total volume 1.5 L) and this suspension stirred for 30 min at room temperature. After demineralization, the insoluble residue was neutralized before being subjected to alkali treatment for deproteination. The neutral alkali insoluble gel was suspended in water (0.8% w/v) and blended for another 10 min. The suspension was stored at 4 °C prior use. Apart from using never dried suspension, parts of the extracts were also freeze-dried for elemental and sugar analysis and density measurements.

2.3. Preparation of chitin nanopapers

Pre-determined amounts of 0.8% (w/v) suspensions from mushroom (stalk, cap, whole) and crab extracts, respectively, were used for nanopaper preparation. Nanopapers with a diameter of 90 mm and a grammage of 2, 5, 10, 20, 40, 80, 160 and 240 g m^{-2} (gsm), respectively, were produced by vacuum filtration on cellulose filter paper (VWR 413, 5-13 μm) in a Büchner funnel. The resulting

filter cake was then wet pressed between blotting papers (3MM CHR blotting paper, VWR) under 5 kg weight to remove excess water before being consolidated in an oven held at 120 °C for 3 h under 5 kg weight. Thereafter, the sample was kept overnight under weight at room temperature to prevent shrinkage during cooling down. For most of the analysis 80 gsm papers were used. The lowest grammage (2 gsm) nanopaper could not be produced by vacuum filtration but was instead prepared by the casting-evaporation method on a polycarbonate petri dish, resulting in a much smoother surface.

2.4. Characterization of ChNF, FChNF and nanopapers

2.4.1. Chemical composition of ChNF and FChNF

Elemental analysis was performed to determine the carbon, hydrogen, nitrogen, sulfur and oxygen content in the freeze-dried extract (EA 1108 CHNS-O, Carlo Erba Instruments, Italy). Carbohydrate analysis was carried out by high performance anion exchange chromatography (HPAEC) to identify the mono-saccharide composition of the extracts. 300 mg freeze-dried sample were mixed with 3 mL 72% sulfuric acid at 30 °C for 60 min. The mixture was then diluted with water to a concentration of 4% and placed in an autoclave at 121 °C for 60 min. HPAEC was performed with a Dionex ICS3000 chromatograph equipped with a CarboPac PA20 column (Dionex, Sunnyvale, CA, USA). Sugar Recovery Standards were prepared and pre-treated under identical hydrolysis conditions prior to HPAEC analysis. The analysis was performed in triplicates.

2.4.2. Morphology of ChNF, FChNF and nanopapers by scanning electron microscopy

The morphology of ChNF, FChNF and nanopapers was investigated by high-resolution field emission scanning electron microscope (SEM) with a LEO Gemini (1525 FEG-SEM, Oberkochen, Germany) at an accelerating voltage of 5 kV. Prior to SEM imaging of the fibre extracts, 3 µL suspension of extracted samples (0.01% w/v) was dropped onto a 400 mesh TEM copper grid attached on carbon tabs and air dried. Samples were chromium coated (K550 sputter coater, Emitech Ltd., Ashford, Kent, UK) for 30 s at 80 mA.

2.4.3. Determination of density, porosity and specific surface area of the nanopapers

The true density (ρ_{true}) of freeze-dried extracts and nanopapers was determined by helium pycnometry (AccuPyc II 1340, Micromeritics, Aachen, Germany) at 23 ± 1 °C. The average of 10 measurement cycles was reported.

The porosity of nanopapers was measured by mercury intrusion porosimetry (AutoPore IV 9500, Micromeritics). The envelope density (ρ_e) of the sample was measured at 0.002 MPa where pores larger than 150 μm were filled by mercury while the skeletal density (ρ_s) was measured at maximum pressure (227 MPa). Given that the limit of mercury penetration into pores for this instrument is 6 nm at maximum pressure, the true porosity of the sample was calculated according to (1)

$$Porosity\ (\%) = \left(1 - \frac{\rho_e}{\rho_{true}}\right) \cdot 100 \qquad (1)$$

where ρ_e is the nanopaper density obtained from mercury intrusion porosimetry, while ρ_{true} is the nanopaper density obtained from helium pycnometry.

Brunauer-Emmett-Teller (BET) specific surface areas of the samples were determined by means of inverse gas chromatography using a surface energy analyzer (SEA, Surface Measurement Systems Ltd., London, UK). Approximately 100 mg freeze-dried powder or 500–700 mg nanopaper were packed in pre-silanized iGC columns (Surface Measurement Systems Ltd., London, UK) and pre-conditioned for 1 h at 30 °C and 0% RH. Helium at a flow rate of 10 sccm was used as a carrier gas and methane was used to determine the dead volume correction factor. The specific BET surface area was measured using octane as probe.

2.4.4. Chemical functionality of ChNF and FChNF nanopapers by IR spectroscopy

ATR-FT-IR spectra of nanopapers were recorded using a Spectrum One FT-IR-spectrometer (Perkin Elmer, Massachusetts, USA). Nanopapers were pressed onto a diamond crystal using a pressure arm and the spectra were collected at a resolution of 2 cm^{-1}, within a range of 600 cm^{-1} and 4000 cm^{-1}. A total of 16 scans was measured and averaged to produce each spectrum.

2.4.5. Mechanical properties of the nanopapers

Mechanical properties of the nanopapers were investigated by dynamic mechanical thermo-analysis (DMTA) and tensile tests. DMTA was conducted in tension mode using a RSA G2 (TA Instruments). Temperature scans were run from 25 °C to 250 °C at a heating rate of 3 °C min^{-1} and a frequency of 1 Hz. Sample dimensions were 15 mm (length) and 5 mm (width). The gauge length used was 10 mm.

Tensile tests were conducted using a TST350 tensile tester (Linkam Scientific Instruments, Surrey, UK) on specimens cut into dog bone shape (overall length 35 mm, narrowest part 2 mm, 10 mm gauge length) using a Zwick cutter. The specimens were secured onto testing cards using a two-part cold curing epoxy resin (Araldite 2011, Huntsman Advanced Materials, Cambridge, UK) prior to the test to prevent damage caused by the clamps. Specimens were conditioned at 27 ± 2 % relative humidity (RH) [52] by storage in a desiccator for at least 24 h. A 200 N load cell was used to test nanopapers at a crosshead speed of 1 mm min^{-1}. The machine compliance (6.38 x 10^{-3} mm N^{-1}) was determined using ASTM C1557-14. Tensile tests were conducted adapting ASTM D638-14. The thicknesses were determined using a handheld microscope on polished epoxy embedded samples, calibrated using 100 x 0.01 mm microscope graticule (Graticules Ltd., Tonbridge, Kent, UK). For each sample a total of 5 specimens were tested.

2.4.6. Characterization of wettability and surface energy

The wettability of nanopapers was characterized by water contact angles using the sessile drop method. Contact angles on the nanopaper surfaces were measured 1 min after placing 10 μL water droplets onto the surface using DSA 10 MK2 (Krüss, Hamburg, Germany). The experiment was conducted at 20 °C and at least five measurements were averaged for each sample.

The critical surface energy (γ_c) of the nanopapers was determined using the wicking method [53]. Rectangular strips (5 mm × 20 mm) were cut from the nanopapers and mounted to one end of a K100 tensiometer (Krüss, Hamburg, Germany) microbalance. The reservoir containing a test liquid was moved upward toward the free end of the strip, and immediately upon contact, the movement of the

reservoir was stopped. The mass gain due to wicking into the nanopaper strip was recorded as function of time. A total of 6 strips was tested for each test liquid. γ_c of the samples was then evaluated using a modified Washburn equation (2):

$$\gamma \cdot \cos\theta = \frac{2}{A^2 r} \cdot \frac{\eta}{\rho^2} \cdot \frac{m^2}{t} \quad (2)$$

where γ, η, ρ, are the surface tension, viscosity and density of the test liquids, respectively. m is the mass gain due to capillarity action (wicking) as function of time t, A and r the average cross-sectional area and radia of the capillaries in the fibrillar network, respectively, and θ the contact angle. In this study, the network geometry of the tested sample is unknown, however, by assuming constant capillary geometry for all nanopapers, the factor $[2/A^2r]$ can be grouped into a constant factor $[1/C]$, which results in (3):

$$C \cdot \gamma \cdot \cos\theta = \frac{\eta}{\rho^2} \cdot \frac{m^2}{t} \quad (3)$$

The critical surface energy of a porous solid, i.e. the nanopaper, can be determined in analogy to a Zisman plot [53]. Here the maximum of the function $[m^2/t][\eta/\rho^2] = f(\gamma)$ corresponds to γ_c and can be determined by performing wicking experiments using a series of different test liquids of known surface tension (Supporting Information Table S1).

Inverse gas chromatography measurements were also performed to determine surface energies on freeze-dried FChNF and nanopapers using a surface energy analyzer (SEA, Surface Measurement Systems Ltd., London, UK). Approximately 100 mg freeze-dried powder or 500–700 mg nanopaper were packed in pre-silanized iGC columns (SMS Ltd., London, UK) and pre-conditioned for 1 h at 30 °C and 0% RH. Helium at a flow rate of 10 sccm was used as a carrier gas and methane was used to determine the dead volume correction factor. The dispersive surface energy component (γ_d) was determined from the net retention volumes of a series of n-alkane probes (hexane, heptane, octane, nonane, and decane) injected at a range of 0.1% to 30% target surface coverages (n/nm). Polar probes (dichloromethane and ethyl acetate) were injected at the same concentrations to determine specific (acid-base) interactions (γ_{ab}). All chromatogram peaks were defined using the first statistical

moment at the peak's center of mass (Peak CoM) of the net retention volumes and surface energies were calculated based on the Schultz method [54].

2.4.7. Surface charge by streaming potential measurements

The surface charge of FChNF nanopapers was investigated using ζ-potential measurements (SurPASS Electrokinetic Analyzer, Anton Paar) based on the streaming potential method using an adjustable gap cell (AGC). For each measurement, a pair of nanopapers (20 mm × 10 mm) was fixed on the rectangular sample holders using double-sided adhesive tape. The sample holders were inserted in the AGC such that the surfaces of the samples were facing each other separated by a gap of approximately 100 μm width. The pH-dependence of the streaming ζ-potential was measured by pumping 1 mM KCl electrolyte solution through the gap with the pH value being set to 10 with 0.1 M KOH and varied between 10 and 2 by titration of 0.1 M HCl using an automatic dual syringe pump system.

3. Results and discussion

Our extraction process yielded 14.0 g of FChNF per kilogram of fresh whole *A. bisporus* (AB); the yields for stalk and cap were 15.4 g $kg^{-1}$and 11.2 g kg^{-1}, respectively. For crab shells, the chitin yield was reported to be 97.2 g kg^{-1} [48]. These variations are expected as mushrooms commonly contain about 94% water. Thus per kg of dry mass mushroom, stalk and cap yielded 254 g and 150 g FChNF, respectively, which is twice as high as for crab, as reported before [48]. It is important to stress that the extraction process of FChNF from AB was very mild in order to preserve the native quality of chitin-based fibres, as an additional acidic treatment can cause removal of glucan [55]. Whereas the extraction of chitin from crustaceans requires prolonged acid treatment for demineralization and deproteination, this was not necessary for the extraction from fungi, due to a lower level of inorganic compounds present [18]. As both demineralization and deproteination steps are known to degrade the chitin chain by hydrolysis and causing partial deacetylation, a higher quality of FChNF was anticipated [51]. Furthermore, no bleaching treatment was carried out due to its known depolymerization effect on the biopolymer chain [36, 56, 57].

The elemental composition of FChNF was determined by elemental analysis and compared to chitin extracted from crab shells and commercially available chitin (see [48]: Supporting information Table S1). The nitrogen content of chitin extracted from crab shells was in accordance with the commercially available one. On the other hand, the nitrogen content of the mushroom extracts was approximately half this value, while the oxygen content was significantly higher. This confirms the presence of glucan which does not contain nitrogen but a higher fraction of hydroxyl groups and thus oxygen.

The ratio between chitin and glucan was determined by carbohydrate analysis (as reported before [48]). From the ratio between glucose (monomer of glucan) and glucosamine (hydrolysis product of chitin) the chitin:glucan ratios determined were 39:61 for stalk and 45:55 for cap, respectively. Denser mycelium packing in the stalk correlates with the higher yield of total fibre mass but the chitin content was higher in the cap [58]. The small amounts of mannose, xylan, and galactose might originate from the water soluble polysaccharide fraction [59, 60] that was entrapped during the extraction process or from residual hemicellulose-like material that cannot be removed during the extraction process. The crab extracts at large resembled the commercial chitin, in which no glucan is present.

Uniform FChNF with 10 to 20 nm in diameter and several μm in length were obtained already directly after chemical extraction of the whole AB (Supporting Information Fig. S1) as also found in a previous study [48]. Further nanofibrillation proved unnecessary as the size of the fibres was already similar to the one attained after grinding [61]. Aggregates of fibrous features were more prevalent in the crab shell extract. After chemical extraction, 10 min post-blending of the crab extract broke the aggregates into nanofibres with an average diameter of 80-120 nm, which is up to six times bigger than the size typically obtained after grinding or homogenizing [62-64]. We were unable to discern the true length of individual fibres due to the high aspect ratio of chitin nanofibres, making it impossible to fit whole fibres in the micrograph without losing resolution, a problem common also with other types of nanofbrils, e.g. cellulose nanofibrils [65]. As far as energy consumption is concerned, being nanosized without undergoing any harsh post-mechanical nanofibrillation signifies

a clear advantage of using mushrooms over crustaceans as source for chitin nanofibers. This might be attributed to the high water content in the mushroom fruiting body (>90%), which renders the structural fibres in the cell wall to be always in a water-swollen state, thus suppressing the hornification effect.

Film formation properties of both ChNF and FChNF were established by dropping and drying suspensions of extracted samples onto a 400 mesh TEM copper grid, observed at low magnification in the SEM. Good film forming capability in contrast to the more disintegrated nature for the animal based ChNF was observed (Fig. 1). This can be ascribed to the presence of amorphous glucan that acts as glue or a polymer matrix binding fibres together in a dense network.

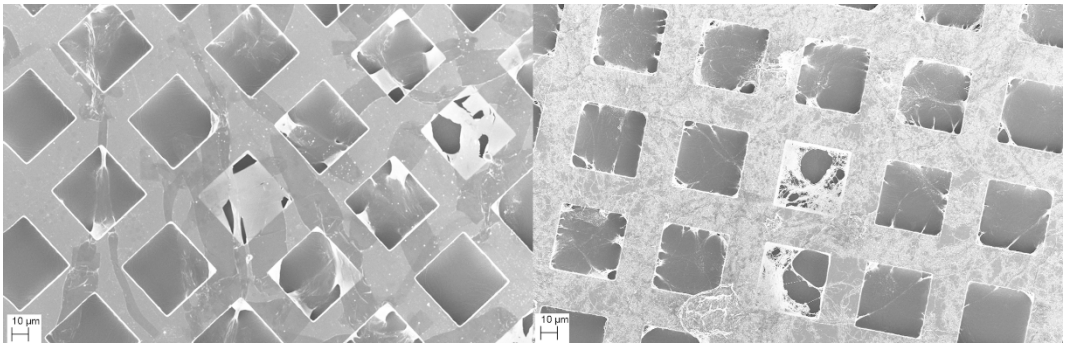

Fig. 1. (left) 0.01% w/v blended whole AB chitin-glucan extract, (right) 0.01% w/v blended pagurus chitin extract.

3.1. Nanopapers from FChNF and ChNF

Surface properties were determined on nanopapers prepared from ChNF and FChNF by vacuum filtration of diluted suspensions of the fibres and subsequent consolidation by heat and pressure. Obvious differences between animal and fungal chitin were observed. Amorphous glucan acted as the cementing material between the fibrils, making the surface of FChNF nanopaper smoother than ChNF nanopaper [48]. This smoothing effect is analogous to the way lignin is being softened during hot pressing, acting as binder to cellulose nanofibrils [66]. Even though both ChNF and FChNF nanopapers had similar density (1.40 and 1.47 g cm^{-3}, respectively) and thus porosity (67 and 59 %, respectively) [48], the FChNF nanopaper (0.22 m^2 g^{-1}) had approximately 8 times lower specific

surface area than the ChNF nanopaper (1.75 m^2 g^{-1}). This again was due to the presence of amorphous glucan that masks the crystalline chitin fibre surface – a feature that can be beneficial e.g. for barrier properties. We should also acknowledge that the presence of mannose in the ChNF sample can contribute to the amorphous character. Nevertheless its content is much lower than that of glucan in the FChNF sample, and thus not really affects the interpretation.

The presence of glucan also affected the mechanical properties of the nanopapers. The evolution of the nanopaper's storage moduli from DMTA in tensile mode across the full temperature range analyzed is depicted in Fig. 2. At room temperature, all samples possessed approximately similar storage moduli between 4 and 6 GPa, with a slight decrease with increasing temperature. This trend continues until about 100 °C, when a drop by two orders of magnitude was observed for the ChNF nanopaper. A similar drop of magnitude was also observed for the FChNF nanopaper but at significantly higher temperatures around 140 °C for stalk and the whole AB nanopaper, and 165 °C for the cap nanopaper, respectively. Chitin supposedly made nanopapers stiffer due to its semi-crystalline structure. The higher chitin content in cap might explain why it retained the modulus at higher temperature compared to the full mushroom or stalk nanopapers. The ChNF nanopaper consisted mostly of chitin, but acid treatment during the extraction process can lead to fibre damage and deacetylation that can compromise the inherent properties of the resulting nanopaper.

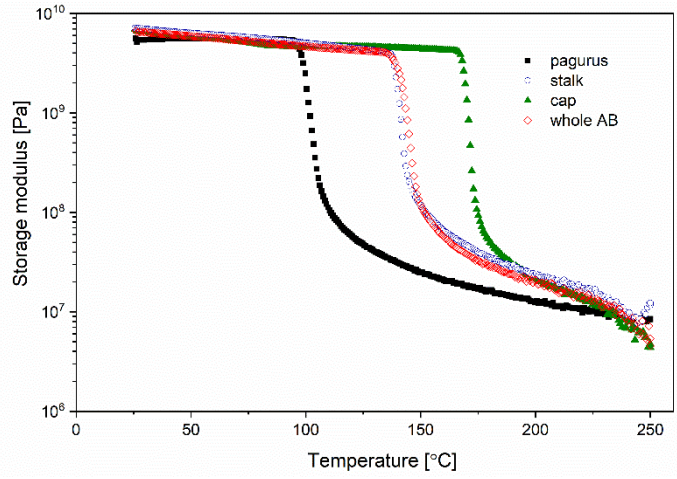

Fig. 2. Evolution of the storage modulus as function of temperature from DMTA.

3.1.1. Chemical functionality of chitin nanopapers by IR spectroscopy

As base for the evaluation of surface properties of chitin nanopapers, the chemical functionality of FChNF and ChNF nanopapers was analyzed by ATR FT-IR spectroscopy (Fig. 3). Both commercial chitin and crab chitin had very similar spectra with a split C=O stretching amide I band at 1620–1670 cm^{-1} that is characteristic for the α-chitin polymorph [67]. This doublet feature could also be observed in fungal chitin spectra but in a convoluted form due to lower crystallinity [48]. The O-H stretching region between 3450 and 3480 cm^{-1} was broader in FChNF compared to ChNF as a result of additional hydroxyl groups present in glucan. It should be noted that the region of the OH-stretch is also heavily influenced by absorbed water which is difficult to eliminate prior to IR measurements. It might be the case that in addition to introducing more hydroxyl groups, amorphous glucan also allowed more water to be absorbed, facilitating a broader OH-band. Similar band broadening was also reported for other mushroom species [61, 68], while well resolved peaks are commonly observed in higher crystalline chitin e.g. from marine algae [69].

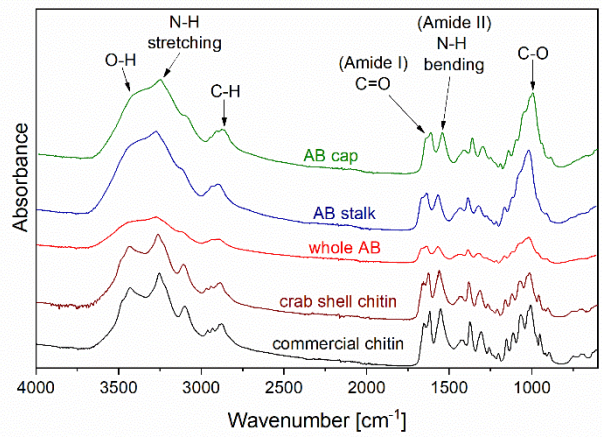

Fig. 3. ATR-FT-IR absorbance of nanopaper sample: bottom to top: commercial chitin, pagurus, stalk, cap, and whole AB, respectively.

3.2. Surface properties of chitin nanopapers

3.2.1. Wettability of chitin nanopapers

The wettability of a material is characterized by its contact angle. Stalk, cap, and AB nanopapers were relatively hydrophobic with water contact angles (~ 65°) almost three times higher than that

(24°) of the ChNF nanopaper (Fig. 4a). Even after 1 h, FChNF nanopapers still retained the shape of a droplet while the water droplets on ChNF nanopapers wicked into the fibre network (Fig. 4b). All nanopapers possessed approximately similar porosity, thus the measured contact angles can be considered to be comparable. By pressing crab chitin whiskers, Nair et al. [70] measured a contact angle as high as 50°. A similar value of 55° was observed for animal chitin films consisting of nanofibres of 10–20 nm in diameter [71]. We suspect that the contact angle of our ChNF nanopaper would fall around these values if higher pressure was applied during nanopaper preparation. However, the values reported in literature were still lower than the contact angle of our FChNF nanopapers.

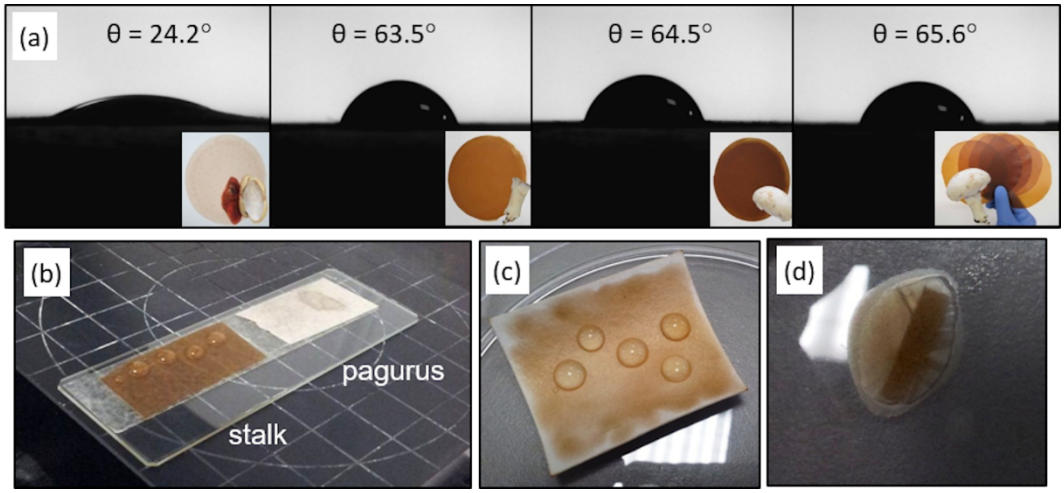

Fig. 4. (a) Water contact angle after 1 min on the nanopapers from (left to right) pagurus, stalk, cap, AB; pictures of water drops after 1 h on (b) stalk and pagurus, (c) AB coated blotting paper, (d) AB coated filter paper.

Reduced hydrophilicity of the FChNF nanopapers was attributed to the lower polarity of the fungal chitin-glucan complex and the lower amount of amine/amide-functionalities present as roughly half of the material in FChNF is glucan. Although additional glucan groups supposedly have increased the hydrophilicity of the nanopapers by adding numerous more accessible hydroxyl groups and by absorbing water, the polar contribution in the ChNF nanopaper was found to be more significant than in the FChNF nanopaper (this will be discussed further below in the inverse gas chromatography section 3.2.3.). The effect of hydrophobin, a unique fungal protein that imparts hydrophobicity to the

fungal mycelium [72] can be ruled out because of the denaturing effect of alkaline treatment toward proteins during the extraction process. The hydrophobic nature of FChNF can be exploited, for example, as a coating agent on an otherwise more hydrophilic material. Fig. 4c shows how a thin coating using 0.8% w/v FChNF prevents water from being absorbed into a blotting paper. The coatings were not only smooth, but also adhered strongly to the surface. When a suspension of FChNF dropped on a small piece of filter paper, formation of a thin FChNF nanopaper is visible around the outer edge (Fig. 4d).

3.2.2. Critical surface tension of chitin nanopapers determined by wicking tests

During wicking tests, FChNF nanopapers absorbed a smaller amount of the test liquid than ChNF nanopapers. Typical wicking curves of formamide into nanopapers are shown in Fig. 5a. The initial slope is a result of the capillary effect imbibing the wetting liquid while the plateau is caused by the balance between capillarity and gravity. By evaluating the initial slopes of the wicking curves, a plot of normalized wicking rate (right hand side of Equation 3) against the surface tension of the test liquids can be computed (Fig. 5b). The data points for each sample are averages from five individual measurements and were fitted using a Gaussian curve. The plot maximum corresponds to Zisman's critical solid-vapor surface tension of the respective nanopaper (γ_c) [73]. Test liquids with surface tension to the left of the maximum fully wet the nanopaper while partial wetting occurs for liquids having surface tensions to the right of the maximum.

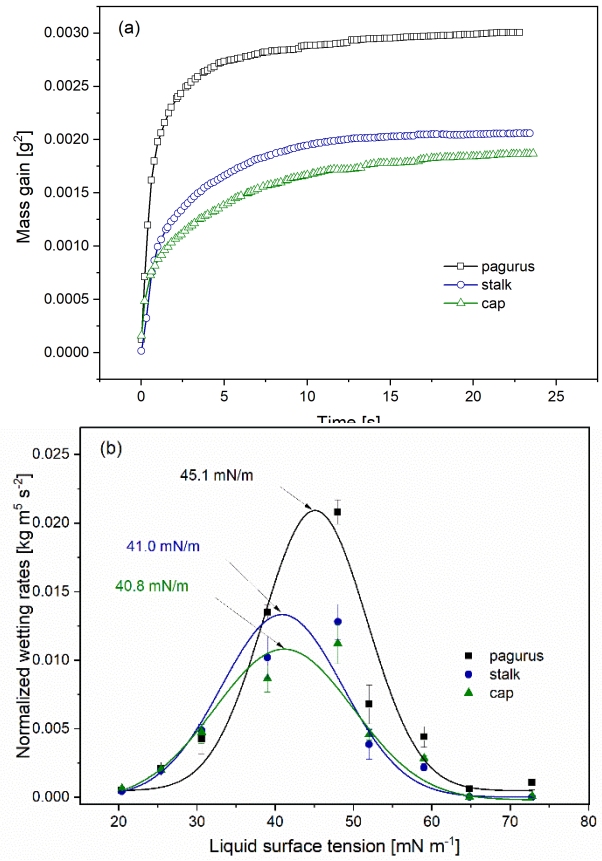

Fig. 5. (a) Typical wicking curve of the nanopapers with formamide, (b) normalized wetting rates as a function of the surface tension of the test liquids.

Stalk and cap FChNF nanopapers had similar γ_c of 41.0 mN m^{-1} and 40.8 mN m^{-1}, respectively, while a higher value of γ_c = 45.1 mN m^{-1} was observed for the ChNF nanopaper. The higher γ_c value of the ChNF nanopaper could be ascribed to its higher crystallinity and lack of glucan [48]. By contrast, the FChNF nanopapers were composite materials consisting of semi-crystalline chitin and amorphous glucan. Hence, the composition of the fungal extract strongly influenced the critical surface tension of the nanopapers.

3.2.3. Surface energy of chitin nanopapers determined by iGC

Surface energy characterization by inverse gas chromatography is traditionally carried out at 'infinite' dilution or near zero surface coverage where only the high energy surface sites are probed. However, a genuine solid surface is often heterogeneous as a result of (i) unevenly distributed disparate functional groups, (ii) the presence of impurities, and/or (iii) irregular surface topography.

A single value at ‘infinite’ dilution will thus only account for a highest surface energy estimate, which is not necessarily representative of the whole material surface. Injecting a larger amount of probe molecules (finite concentration) allows for more interaction to be established between the probe molecule and low surface energy sites of the sample, hence allowing a surface heterogeneity profile to be plotted [74].

Fig. 6 illustrates the surface energy profiles for chitin nanopapers measured by inverse gas chromatography. The values of dispersive surface energy (γ_d), acid-base surface energy (γ_{ab}), and total surface energy (γ_t) at ‘infinite’ dilution (n/nm = 0.01) are summarized in Table 1. The decreasing value of surface energy with increasing surface coverage was due to interaction with less energetic sites and the upper limit of n/nm = 0.3 was chosen to rule out vapor-vapor interaction that can occur at higher surface coverage.

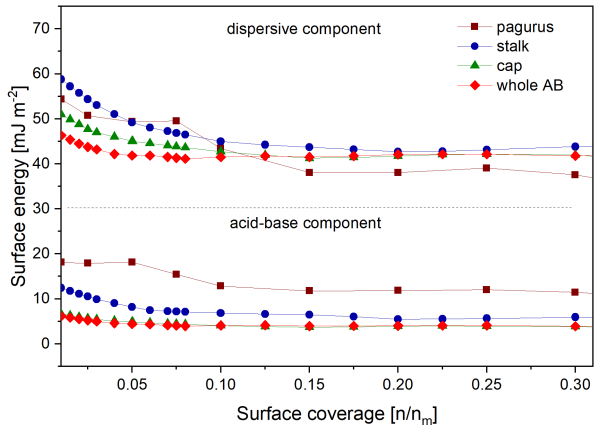

Fig. 6. Surface energy profiles for chitin nanopapers as measured by inverse gas chromatography.

Table 1. Dispersive surface energy (γ_d), acid-base surface energy (γ_{ab}), and total surface energy (γ_t) at infinite dilution (n/nm = 0.01) for nanopapers and freeze-dried powder samples.

Sample	γ_d [mJ m^{-2}]		γ_{ab} [mJ m^{-2}]		γ_t [mJ m^{-2}]	
	powder	nanopaper	powder	nanopaper	powder	nanopaper
Pagurus	47.3	54.4	10.2	18.1	57.5	72.5
Stalk	46.2	58.8	6.7	12.4	52.9	71.2
Cap	41.8	51.0	6.2	6.7	48.0	57.7
AB	38.8	46.3	5.7	6.2	44.5	52.5

Our freeze-dried sample was first powdered using non-cryogenic milling in order to facilitate their insertion into the iGC column. Intense milling activity generally increases γ_d due to the formation of higher energy amorphous surfaces [75], but a decrease in γ_d is also possible if a lower energy surface was exposed during the process [76]. Low intensive milling adopted in this study (3 min, 1 cycle) should not have markedly altered the surface energy of the powdered sample. The dispersive surface energy of ChNF chitin was γ_d = 47.3 mJ m^{-2}. This was significantly higher than what has been reported in literature for crustacean chitin: γ_d = 37–41 mJ m^{-2} [77-79]. The disparity can be explained by the different processing and drying techniques used. iGC results reported for chitin so far used commercial chitin that has been heat-dried, thus the difference in the surface energy was expected. Severe fibre collapse during the heat treatment reduces the overall surface area, hence, obstructing potential exposure of the more active sites. In addition, our measurement performed at 0% RH reduces the occupation of higher energy adsorption sites by water molecules, thus resulting in a higher total surface energy value.

All powdered samples exhibited lower γ_d than the nanopapers due to their lower crystallinity [48]. Stalk, which possesses the largest difference in crystallinity between powder and nanopaper, had the highest γ_d difference of 12.6 mJ m^{-2}. ChNF, on the other hand, exhibited the smallest γ_d difference (7.1 mJ m^{-2}) between powder and nanopaper, which indicates the modest crystallinity difference between the two forms.

The nanopaper surface was also found to be more heterogeneous in surface energy than the powder surface. Among the FChNF nanopapers, the stalk nanopaper had the most heterogeneous surface profile with a difference between the highest energy site and the lowest energy site as large as 16.1 mJ m^{-2}. In comparison, cap and AB nanopapers had a difference of only 8.8 mJ m^{-2} and 4.1 mJ m^{-2}, respectively. A similar trend in heterogeneity (stalk > cap >AB) was also observed for the powders. A higher fibre anisotropy in stalk, presumably longer and more oriented fibres, could be the reason for their more heterogeneous γ_d profile.

The relatively high value of γ_{ab} in the ChNF sample was attributed to a higher content of polar amine and amide groups, which, in the case of FChNF samples, was lower due to the presence of glucan.

The hydroxyl groups on glucan are less polar than the amine/amide groups on chitin. Higher surface polarity not only caused the ChNF nanopaper to be more hydrophilic as evidenced by measured water contact angles, but also increased its total surface energy. As a result, the ChNF sample had a higher γ_t than the FChNF sample. It is worth noting that the polar component of the surface energy is much more complex and there are many factors that influence the polarity other than just the amount of hydroxyl and amine/amide groups. The way the amine/amide and hydroxyl groups are exposed in the chitin crystal is crucial, for example.

3.2.4. Surface charge of chitin nanopapers

ζ-potential measurements provide information on the surface chemistry of a solid material when it is in contact with an aqueous electrolyte solution. The dissociation behavior of surface functional groups across a pH range can give an indication of surface Brønsted basicity or acidity of the tested material [80]. Fig. 7 shows the streaming ζ-potential of ChNF, stalk, cap and AB nanopaper as a function of pH.

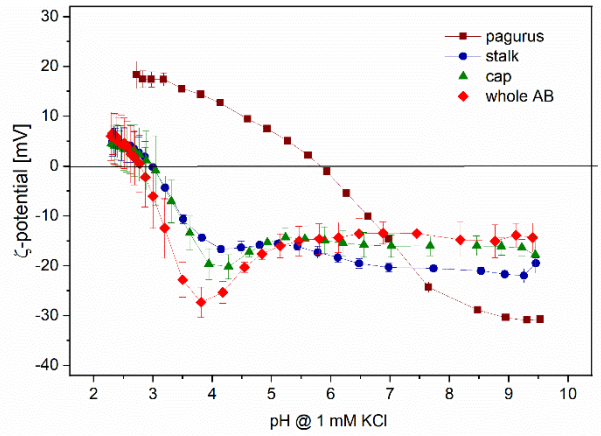

Fig. 7. Streaming ζ-potential of chitin nanopapers as a function of pH.

All FChNF nanopapers exhibited a plateau at neutral and high pH, indicating that the surface was acidic as all dissociable functional groups were fully deprotonated. The acidic character was due to carboxyl groups present in the glucan and chitin backbones. Identical isoelectric points (iep) at pH 3 for the different FChNF nanopapers indicated similar charged surface groups for stalk, cap and AB. The slightly lower plateau observed in stalk ($\zeta_{plateau}$ = −20 mV) compared to cap or AB ($\zeta_{plateau}$ = −14

to −15 mV) was ascribed to a lower amount of carboxylic acid groups present in additional pigmentation compounds existing in cap gill. The absence of gill pigment consequently improves the accessibility of dissociable acidic groups in the stalk nanopaper.

The ChNF nanopaper exhibited a sigmoidal ζ = f(pH) curve which indicated an amphoteric surface character due to the partial deacetylation of N-acetylglucosamine moieties in ChNF fibrils caused by the alkaline and acidic treatment. The protonation of the free amine groups in partially deacetylated chitin imparted a positive surface charge on the ChNF nanopaper surface, as exemplified by the positive value of ζ-potential in the broad acidic region below pH 6 (iep = 5.8). By contrast, in the FChNF nanopapers the fraction of free amine groups was much lower due to (i) the coverage of chitin by grafted glucan, i.e. the lower relative prevalence of chitin, for glucan substituting about half of the chitin in FChNF and (ii) milder extraction procedures causing less deacetylation. Positive ζ-potential at very low pH occurred not because of amine group protonation but rather because of adsorption of protons (H_3O^+) on the nanopaper surface. The more negative plateau at high pH observed for the ChNF nanopaper ($\zeta_{plateau}$ = −30 mV) compared to the FChNF nanopaper ($\zeta_{plateau}$ = −14 to −20 mV) at higher pH was attributed to a higher fraction of acidic groups in chitin exposed to the surface also caused by higher crystallinity of ChNF nanopapers [48]. Furthermore, the presence of amorphous glucan in FChNF nanopapers promoted swelling in water. This swelling in turn caused the transfer of the plane of shear into the electrolyte which excludes the diffusive part of the electric double layer from mechanical and electrical interaction [81], consequently reducing the ζ-potential toward 0 mV.

3.3. Influence of grammage/thickness on the properties of FChNF nanopapers

Papers with grammages of 2, 5, 10, 20, 40, 80, 160 and 240 gsm were prepared (Fig. 8). Optically, all nanopapers between 2 and 160 gsm were transparent against a background. Even the nanopaper with the highest grammage (240 gsm) and thus thickness (~200 μm) was found to be translucent. These good optical properties could be ascribed to the small size of the nanofibrils and the smooth surface of the resulting nanopapers, which reduced the effect of light scattering. The residual golden

color of the nanopapers is a by-product of a pigment compound not removed during the mild extraction process.

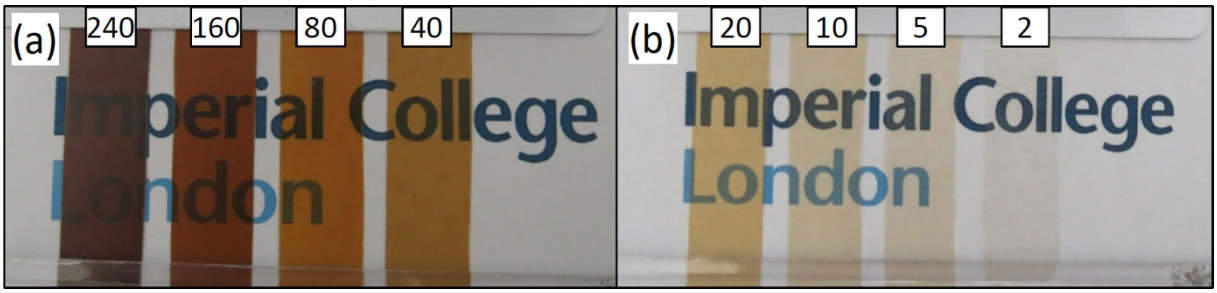

Fig. 8 Appearance of AB nanopapers against background; the numbers represent the grammage [gsm].

The influence of the grammage of the nanopapers on the mechanical properties was evaluated by tensile tests. The grammage and thus thickness of FChNF nanopapers significantly influenced their mechanical properties (Fig. 9). The tensile strength as function of grammage was not straightforward because the tensile strength is affected by the number of defects in a sample. More defects will cause lower tensile strength. The probability of defects such as microcracks is greater when cutting a thicker sample. A similar trend was reported by I'Anson et al. [82, 83]. They attributed the decrease of tensile strength to an increased probability of weak points in the fibre network with an increasing sample volume. However, the chance of defects such as pinholes being responsible for fracture is higher at lower grammage. Hence, the two effects were competing resulting in an optimal grammage for tensile strength of 80 gsm, as also found before [48].

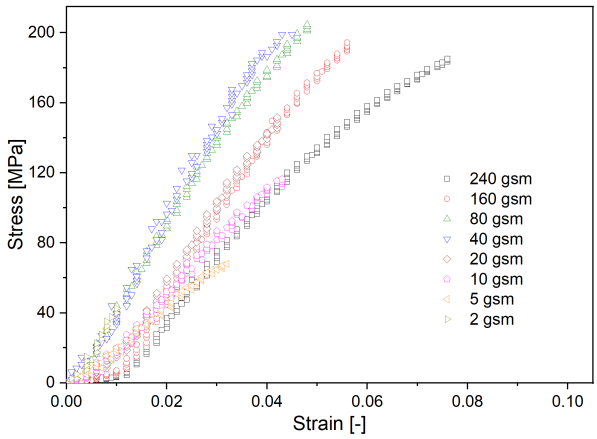

Fig. 9. Stress-strain curves of AB nanopapers with different grammage. Data for 80 gsm was taken from [48].

The nanopaper density (Fig. 10) at different grammage was not responsibility for this trend as it did not vary (see Section 3.1.). However, at low grammage (2 to 40 gsm), the specific tensile strength increased with increasing grammage, reaching a maximum between 40 and 80 gsm before gradually decreasing at 160 and 240 gsm. On the other hand, the Young's modulus steadily increased with increasing grammage. This is based on the fact that the modulus is a material property and thus less sensitive to defects.

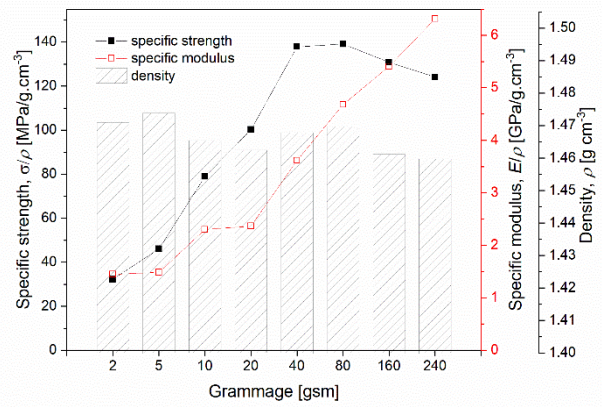

Fig. 10. Evolution of specific strength, specific modulus and density as a function of grammage.

iGC was performed to evaluate the impact of grammage on the surface energy. It was found that higher grammage nanopapers (80 to 240 gsm) had slightly higher dispersive surface energy (γ_d) than lower grammage nanopapers (Fig. 11a). This is in particular true for surface coverages n/nm > 0.1. With a γ_d of 40 mJ m^{-2}, 2 gsm nanopapers had the fewest active sites on its surface and hence lowest surface energy. It was also energetically less heterogeneous compared to all the other nanopapers – a side-effect of the smoother surface generated by the slow casting-evaporation process. Little variation of the acid-base component of the surface energy (< 2 mJ m^{-2}) with grammage was observed at surface coverages n/nm > 0.1, indicating that similar functional groups are exposed on all nanopaper surfaces.

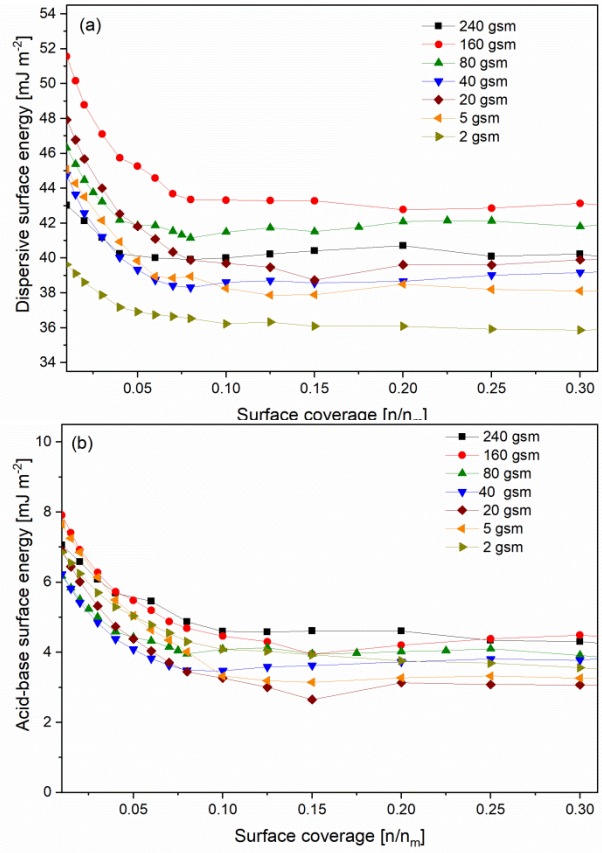

Fig. 11. (a) Dispersive surface energy profile and (b) acid-base surface energy profile for FChNF nanopapers with different grammages as measured by iGC.

4. Conclusions

Fungal chitin nanofibers (FChNFs) were extracted from *Agaricus bisporus*, i.e. common white button mushroom, and used for the preparation of nanopapers. One kg dry mass of the raw biomass yielded about 200 g chitin-glucan composite fibres, which is approx. double the amount of chitin fibres that could be extracted per kg crab shells. The presence of glucan in FChNF was confirmed by elemental analysis, sugar analysis and FT-IR spectroscopy. The primary goal of this study was to elucidate the impact of glucan onto the surface properties of chitin nanopapers prepared from fungi extract. FChNF nanopapers had a significantly lower water wettability compared to ChNF nanopapers derived from crab shells. The lower wettability was due to the lower surface tension/energy of FChN as confirmed by wicking test and inverse gas chromatography. Higher surface energy of ChNF nanopapers indicated higher polarity due to the greater abundance of

amine/amide groups on the surface of the nanopapers. ChNF nanopapers were amphoteric with an iep of 5.8 indicating the presence of both amine and acidic groups, whereas FChNF nanopapers in which the chitin was buried in a glucan matrix exhibited an acidic surface character as indicated by the iep of 3. All these surface properties have a tremendous impact onto the applicability of the material and hence potential applications. The presence of glucan improved film formation properties resulting in much better mechanical properties of FChNF nanopapers as compared to ChNF nanopapers. Moreover, FChNF nanopapers were more hydrophobic. Ultimately, it was demonstrated that the chitin-glucan complex extracted from fungal biomass is not just an alternative to animal chitin, in particular when used in film or nanopaper form, but the possibility to control surface properties, for instance by growing conditions of mushrooms and/or species and/or extraction protocols, opens up a wide range of further applications.

Acknowledgements

The authors thank Johannes Theiner (Mikroanalytisches Laboratorium, Faculty of Chemistry, University of Vienna) for elemental analysis. WMFWN was supported by the International Islamic University Malaysia and Ministry of Education Malaysia. Funding of AM by the University of Vienna is also acknowledged.

References

[1] R. Xiong, A.M. Grant, R. Ma, S. Zhang, V.V. Tsukruk, Naturally-derived biopolymer nanocomposites: Interfacial design, properties and emerging applications, Mater. Sci. Eng., R, 125 (2018) 1-41.

[2] K.-Y. Lee, Y. Aitomäki, L.A. Berglund, K. Oksman, A. Bismarck, On the use of nanocellulose as reinforcement in polymer matrix composites, Compos. Sci. Technol., 105 (2014) 15-27.

[3] S.J. Eichhorn, A. Dufresne, M. Aranguren, N.E. Marcovich, J.R. Capadona, S.J. Rowan, C. Weder, W. Thielemans, M. Toman, S. Renneckar, W. Gindl, S. Veigel, J. Keckes, H. Yano, K. Abe, M. Nogi, A.N. Nakagaito, A. Mangalam, J. Simonsen, A.S. Benight, A. Bismarck, L.A. Berglund, T. Peijs, Review: current international research into cellulose nanofibres and nanocomposites, J. Mater. Sci., 45 (2010) 1-33.

[4] D. Klemm, F. Kramer, S. Moritz, T. Lindstroem, M. Ankerfors, D. Gray, A. Dorris, Nanocelluloses: A New Family of Nature-Based Materials, Angew. Chem. Int. Ed., 50 (2011) 5438-5466.

[5] K. Oksman, Y. Aitomäki, A.P. Mathew, G. Siqueira, Q. Zhou, S. Butylina, S. Tanpichai, X. Zhou, S. Hooshmand, Review of the recent developments in cellulose nanocomposite processing, Composites Part A, 83 (2016) 2-18.

[6] A. Mautner, K.-Y. Lee, P. Lahtinen, M. Hakalahti, T. Tammelin, K. Li, A. Bismarck, Nanopapers for organic solvent nanofiltration, Chem. Commun., 50 (43) (2014) 5778-5781.

[7] G. Metreveli, L. Wågberg, E. Emmoth, S. Belák, M. Strømme, A. Mihranyan, A Size-Exclusion Nanocellulose Filter Paper for Virus Removal, Adv. Healthc. Mater., 3 (10) (2014) 1546-1550.

[8] A. Mautner, K.-Y. Lee, T. Tammelin, A.P. Mathew, A.J. Nedoma, K. Li, A. Bismarck, Cellulose nanopapers as tight aqueous ultra-filtration membranes, React. Funct. Polym., 86 (2015) 209-214.

[9] A. Mautner, J. Lucenius, M. Österberg, A. Bismarck, Multi-layer nanopaper based composites, Cellulose, 24 (4) (2017) 1759-1773.

[10] A.N. Nakagaito, S. Iwamoto, H. Yano, Bacterial cellulose: the ultimate nano-scalar cellulose morphology for the production of high-strength composites, Appl. Phys. A, 80 (1) (2005) 93-97.

[11] M. Nogi, H. Yano, Transparent Nanocomposites Based on Cellulose Produced by Bacteria Offer Potential Innovation in the Electronics Device Industry, Adv. Mater., 20 (10) (2008) 1849-1852.

[12] F. Ansari, S. Galland, M. Johansson, C.J.G. Plummer, L.A. Berglund, Cellulose nanofiber network for moisture stable, strong and ductile biocomposites and increased epoxy curing rate, Composites Part A, 63 (2014) 35-44.

[13] M. Henriksson, L. Fogelström, L.A. Berglund, M. Johansson, A. Hult, Novel nanocomposite concept based on cross-linking of hyperbranched polymers in reactive cellulose nanopaper templates, Compos. Sci. Technol., 71 (1) (2011) 13-17.

[14] H. Braconnot, Sur la nature des champignons, Ann. Chim. Phys., 79 (2) (1811) 265-304.

[15] J.G. Children, On the nature of mushrooms, Zoo. Journal, 1 (1824) 101-111.

[16] A. Payen, C.R. Hebd, Mémoire sur la composition du tissu propre des plantes et du ligneux., Seances Acad. Sci., 7 (1838a) 1052-1056.

[17] M. Rinaudo, Chitin and chitosan: Properties and applications, Prog. Polym. Sci., 31 (7) (2006) 603-632.

[18] R.A.A. Muzzarelli, Chitin Nanostructures in Living Organisms, in: N.S. Gupta (Ed.) Chitin: Formation and Diagenesis, Springer Netherlands, Dordrecht, 2011, pp. 1-34.

[19] R.A.A. Muzzarelli, E.R. Pariser, Proceedings of 1st International Conference on Chitin/Chitosan, MIT Sea Grant Program 78-7, Cambridge, Mass., 1978.

[20] S. Kataoka, T. Ando, Regenerated Chitin Film from the Solution of Trichloroacetic Acid Systems, Kobunshi Ronbunshu, 36 (3) (1979) 175-181.

[21] N.L.B.M. Yusof, L.Y. Lim, E. Khor, Flexible chitin films: structural studies, Carbohydr. Res., 339 (16) (2004) 2701-2711.

[22] S. Ifuku, S. Morooka, A. Norio Nakagaito, M. Morimoto, H. Saimoto, Preparation and characterization of optically transparent chitin nanofiber/(meth)acrylic resin composites, Green Chem., 13 (7) (2011) 1708-1711.

[23] J.-I. Kadokawa, A. Takegawa, S. Mine, K. Prasad, Preparation of chitin nanowhiskers using an ionic liquid and their composite materials with poly(vinyl alcohol), Carbohydr. Polym., 84 (4) (2011) 1408-1412.

[24] Y. Fan, H. Fukuzumi, T. Saito, A. Isogai, Comparative characterization of aqueous dispersions and cast films of different chitin nanowhiskers/nanofibers, Int. J. Biol. Macromol., 50 (1) (2012) 69-76.

[25] N. Ezekiel Mushi, N. Butchosa, Q. Zhou, L.A. Berglund, Nanopaper membranes from chitin–protein composite nanofibers—structure and mechanical properties, J. Appl. Polym. Sci., 131 (7) (2013).

[26] B. Duan, C. Chang, B. Ding, J. Cai, M. Xu, S. Feng, J. Ren, X. Shi, Y. Du, L. Zhang, High strength films with gas-barrier fabricated from chitin solution dissolved at low temperature, J. Mater. Chem. A, 1 (5) (2013) 1867-1874.

[27] S. Ifuku, A. Ikuta, H. Izawa, M. Morimoto, H. Saimoto, Control of mechanical properties of chitin nanofiber film using glycerol without losing its characteristics, Carbohydr. Polym., 101 (2014) 714-717.

[28] P. Hassanzadeh, W. Sun, J.P. de Silva, J. Jin, K. Makhnejia, G.L.W. Cross, M. Rolandi, Mechanical properties of self-assembled chitin nanofiber networks, J. Mater. Chem. B, 2 (17) (2014) 2461-2466.

[29] N.E. Mushi, S. Utsel, L.A. Berglund, Nanostructured biocomposite films of high toughness based on native chitin nanofibers and chitosan, Front. Chem, 2 (2014) 99-99.

[30] J. Jin, D. Lee, H.-G. Im, Y.C. Han, E.G. Jeong, M. Rolandi, K.C. Choi, B.-S. Bae, Chitin Nanofiber Transparent Paper for Flexible Green Electronics, Adv. Mater., 28 (26) (2016) 5169-5175.

[31] M. Kaya, I. Sargin, I. Sabeckis, D. Noreikaite, D. Erdonmez, A.M. Salaberria, J. Labidi, V. Baublys, V. Tubelytė, Biological, mechanical, optical and physicochemical properties of natural chitin films obtained from the dorsal pronotum and the wing of cockroach, Carbohydr. Polym., 163 (2017) 162-169.

[32] M.G. Casteleijn, D. Richardson, P. Parkkila, N. Granqvist, A. Urtti, T. Viitala, Spin coated chitin films for biosensors and its analysis are dependent on chitin-surface interactions, Colloids Surf., A, 539 (2018) 261-272.

[33] M. Kaya, A.M. Salaberria, M. Mujtaba, J. Labidi, T. Baran, P. Mulercikas, F. Duman, An inclusive physicochemical comparison of natural and synthetic chitin films, Int. J. Biol. Macromol., 106 (2018) 1062-1070.

[34] K. Kim, M. Ha, B. Choi, S.H. Joo, H.S. Kang, J.H. Park, B. Gu, C. Park, C. Park, J. Kim, S.K. Kwak, H. Ko, J. Jin, S.J. Kang, Biodegradable, electro-active chitin nanofiber films for flexible piezoelectric transducers, Nano Energy, 48 (2018) 275-283.

[35] G.G. Allan, J.R. Fox, N. Kong, A critical evaluation of the potential sources of chitin and chitosan, in: R.A.A. Muzzarelli, E.R. Pariser (Eds.) Proceedings of 1st International Conference on Chitin/Chitosan, MIT Sea Grant Program 78-7, Cambridge, Mass., 1978, pp. 64-78.

[36] J.H. Sietsma, J.G.H. Wessels, Evidence for Covalent Linkages between Chitin and β-Glucan in a Fungal Wall, Microbiology, 114 (1) (1979) 99-108.

[37] R. Surarit, M.G. Gopal Pk Fau - Shepherd, M.G. Shepherd, Evidence for a glycosidic linkage between chitin and glucan in the cell wall of Candida albicans, J. Gen. Microbiol., 134 (1988) 1723-1730.

[38] R. Kollar, B.B. Reinhold, E. Petrakova, H.J. Yeh, G. Ashwell, J. Drgonova, J.C. Kapteyn, F.M. Klis, E. Cabib, Architecture of the yeast cell wall. Beta(1-->6)-glucan interconnects mannoprotein, beta(1-->)3-glucan, and chitin, J. Biol. Chem., 272 (28) (1997) 17762-17775.

[39] R.P. Hartland, C.A. Vermeulen, J.H. Sietsma, J.G.H. Wessels, F.M. Klis, The linkage of (1–3)-β-glucan to chitin during cell wall assembly in Saccharomyces cerevisiae, Yeast, 10 (12) (1994) 1591-1599.

[40] L. Heux, J. Brugnerotto, J. Desbrières, M.F. Versali, M. Rinaudo, Solid State NMR for Determination of Degree of Acetylation of Chitin and Chitosan, Biomacromolecules, 1 (4) (2000) 746-751.

[41] T. Fontaine, C. Simenel, G. Dubreucq, O. Adam, M. Delepierre, J. Lemoine, C.E. Vorgias, M. Diaquin, J.P. Latgé, Molecular organization of the alkali-insoluble fraction of Aspergillus fumigatus cell wall, J. Biol. Chem., 275 (36) (2000) 27594-27607.

[42] T. Stalhberger, C. Simenel, C. Clavaud, V.G.H. Eijsink, R. Jourdain, M. Delepierre, J.-P. Latgé, L. Breton, T. Fontaine, Chemical Organization of the Cell Wall Polysaccharide Core of Malassezia restricta, J. Biol. Chem., 289 (18) (2014) 12647-12656.

[43] J. Janesch, M. Jones, M. Bacher, E. Kontturi, A. Bismarck, A. Mautner, Mushroom-derived chitosan-glucan nanopaper filters for the treatment of water, React. Funct. Polym., 146 (2019) 104428.

[44] A.L. Lopata, R.E. O'Hehir, S.B. Lehrer, Shellfish allergy, Clin. Exp. Allergy, 40 (6) (2010) 850-858.

[45] M.-F. Versali, F. Clerisse, J.-M. Bruyere, S. Gautier, in, US, 2009.

[46] EFSA Panel on Dietetic Products, Nutrition and Allergies (NDA), Scientific Opinion on the safety of 'Chitin-glucan' as a Novel Food ingredient, EFSA Journal, 8 (7) (2010) 1687.

[47] E. Khor, Chapter 1 - The Relevance of Chitin, in: E. Khor (Ed.) Chitin, Elsevier Science Ltd, Oxford, 2001, pp. 1-8.

[48] W.M. Fazli Wan Nawawi, K.-Y. Lee, E. Kontturi, R.J. Murphy, A. Bismarck, Chitin Nanopaper from Mushroom Extract: Natural Composite of Nanofibers and Glucan from a Single Biobased Source, ACS Sustain. Chem. Eng., 7 (7) (2019) 6492-6496.

[49] M. Jones, K. Weiland, M. Kujundzic, J. Theiner, H. Kählig, E. Kontturi, S. John, A. Bismarck, A. Mautner, Waste-Derived Low-Cost Mycelium Nanopapers with Tunable Mechanical and Surface Properties, Biomacromolecules, 20 (9) (2019) 3513-3523.

[50] H.K. No, S.P. Meyers, K.S. Lee, Isolation and characterization of chitin from crawfish shell waste, J. Agric. Food. Chem., 37 (3) (1989) 575-579.

[51] A. Percot, C. Viton, A. Domard, Optimization of Chitin Extraction from Shrimp Shells, Biomacromolecules, 4 (1) (2003) 12-18.

[52] D.N.S. Hon, Cellulose: a random walk along its historical path, Cellulose, 1 (1) (1994) 1-25.

[53] J. Tröger, K. Lunkwitz, K. Grundke, W. Bürger, Determination of the surface tension of microporous membranes using wetting kinetics measurements, Colloids Surf., A, 134 (3) (1998) 299-304.

[54] J. Schultz, L. Lavielle, C. Martin, The Role of the Interface in Carbon Fibre-Epoxy Composites, J. Adhesion, 23 (1) (1987) 45-60.

[55] A. Hassainia, H. Satha, S. Boufi, Chitin from Agaricus bisporus: Extraction and characterization, Int. J. Biol. Macromol., 117 (2018) 1334-1342.

[56] T. Topalovic, V.A. Nierstrasz, L. Bautista, D. Jocic, A. Navarro, M.M.C.G. Warmoeskerken, Analysis of the effects of catalytic bleaching on cotton, Cellulose, 14 (4) (2007) 385-400.

[57] S. Jolivet, N. Arpin, H.J. Wichers, G. Pellon, Agaricus bisporus browning: a review, Mycol. Res., 102 (12) (1998) 1459-1483.

[58] J. Vetter, Chitin content of cultivated mushrooms Agaricus bisporus, Pleurotus ostreatus and Lentinula edodes, Food Chem., 102 (1) (2007) 6-9.

[59] A. Patyshakuliyeva, E. Jurak, A. Kohler, A. Baker, E. Battaglia, W. de Bruijn, K.S. Burton, M.P. Challen, P.M. Coutinho, D.C. Eastwood, B.S. Gruben, M.R. Mäkelä, F. Martin, M. Nadal, J. van den Brink, A. Wiebenga, M. Zhou, B. Henrissat, M. Kabel, H. Gruppen, R.P. de Vries, Carbohydrate utilization and metabolism is highly differentiated in Agaricus bisporus, BMC Genomics, 14 (1) (2013) 663.

[60] F.R. Smiderle, A.C. Ruthes, J. van Arkel, W. Chanput, M. Iacomini, H.J. Wichers, L.J.L.D. Van Griensven, Polysaccharides from Agaricus bisporus and Agaricus brasiliensis show similarities in their structures and their immunomodulatory effects on human monocytic THP-1 cells, BMC Complement. Altern. Med., 11 (1) (2011) 58.

[61] S. Ifuku, R. Nomura, M. Morimoto, H. Saimoto, Preparation of Chitin Nanofibers from Mushrooms, Materials, 4 (8) (2011).

[62] S. Ifuku, M. Nogi, K. Abe, M. Yoshioka, M. Morimoto, H. Saimoto, H. Yano, Simple preparation method of chitin nanofibers with a uniform width of 10–20nm from prawn shell under neutral conditions, Carbohydr. Polym., 84 (2) (2011) 762-764.

[63] S. Ifuku, M. Nogi, M. Yoshioka, M. Morimoto, H. Yano, H. Saimoto, Fibrillation of dried chitin into 10–20nm nanofibers by a simple grinding method under acidic conditions, Carbohydr. Polym., 81 (1) (2010) 134-139.

[64] S. Ifuku, M. Nogi, K. Abe, M. Yoshioka, M. Morimoto, H. Saimoto, H. Yano, Preparation of Chitin Nanofibers with a Uniform Width as α-Chitin from Crab Shells, Biomacromolecules, 10 (6) (2009) 1584-1588.

[65] W. Chen, Q. Li, J. Cao, Y. Liu, J. Li, J. Zhang, S. Luo, H. Yu, Revealing the structures of cellulose nanofiber bundles obtained by mechanical nanofibrillation via TEM observation, Carbohydr. Polym., 117 (2015) 950-956.

[66] E. Rojo, M.S. Peresin, W.W. Sampson, I.C. Hoeger, J. Vartiainen, J. Laine, O.J. Rojas, Comprehensive elucidation of the effect of residual lignin on the physical, barrier, mechanical and surface properties of nanocellulose films, Green Chem., 17 (3) (2015) 1853-1866.

[67] P. Sikorski, R. Hori, M. Wada, Revisit of α-Chitin Crystal Structure Using High Resolution X-ray Diffraction Data, Biomacromolecules, 10 (5) (2009) 1100-1105.

[68] T. Wu, S. Zivanovic, F.A. Draughon, W.S. Conway, C.E. Sams, Physicochemical Properties and Bioactivity of Fungal Chitin and Chitosan, J. Agric. Food. Chem., 53 (10) (2005) 3888-3894.

[69] Y. Ogawa, S. Kimura, M. Wada, S. Kuga, Crystal analysis and high-resolution imaging of microfibrillar α-chitin from Phaeocystis, J. Struct. Biol., 171 (1) (2010) 111-116.

[70] K. Gopalan Nair, A. Dufresne, A. Gandini, M.N. Belgacem, Crab Shell Chitin Whiskers Reinforced Natural Rubber Nanocomposites. 3. Effect of Chemical Modification of Chitin Whiskers, Biomacromolecules, 4 (6) (2003) 1835-1842.

[71] M.I. Shams, S. Ifuku, M. Nogi, T. Oku, H. Yano, Fabrication of optically transparent chitin nanocomposites, Appl. Phys. A, 102 (2) (2011) 325-331.

[72] J.G.H. Wessels, Hydrophobins: Proteins that Change the Nature of the Fungal Surface, Adv. Microb. Physiol., 38 (1996) 1-45.

[73] A. Baltazar-y-Jimenez, A. Bismarck, Wetting behaviour, moisture up-take and electrokinetic properties of lignocellulosic fibres, Cellulose, 14 (2) (2007) 115-127.

[74] P.P. Ylä-Mäihäniemi, J.Y.Y. Heng, F. Thielmann, D.R. Williams, Inverse Gas Chromatographic Method for Measuring the Dispersive Surface Energy Distribution for Particulates, Langmuir, 24 (17) (2008) 9551-9557.

[75] U.V. Shah, D. Olusanmi, A.S. Narang, M.A. Hussain, M.J. Tobyn, S.J. Hinder, J.Y.Y. Heng, Decoupling the Contribution of Surface Energy and Surface Area on the Cohesion of Pharmaceutical Powders, Pharm. Res., 32 (1) (2015) 248-259.

[76] R. Ho, M. Naderi, J.Y.Y. Heng, D.R. Williams, F. Thielmann, P. Bouza, A.R. Keith, G. Thiele, D.J. Burnett, Effect of Milling on Particle Shape and Surface Energy Heterogeneity of Needle-Shaped Crystals, Pharm. Res., 29 (10) (2012) 2806-2816.

[77] A.G. Cunha, S.C.M. Fernandes, C.S.R. Freire, A.J.D. Silvestre, C.P. Neto, A. Gandini, What Is the Real Value of Chitosan's Surface Energy?, Biomacromolecules, 9 (2) (2008) 610-614.

[78] B. Shi, S. Zhao, L. Jia, L. Wang, Surface characterization of chitin by inverse gas chromatography, Carbohydr. Polym., 67 (3) (2007) 398-402.

[79] M.N. Belgacem, A. Blayo, A. Gandini, Surface Characterization of Polysaccharides, Lignins, Printing Ink Pigments, and Ink Fillers by Inverse Gas Chromatography, J. Colloid Interface Sci., 182 (2) (1996) 431-436.

[80] A. Bismarck, M. Pfaffernoschke, M. Selimović, J. Springer, Electrokinetic and contact angle measurements of grafted carbon fibers, Colloid. Polym. Sci., 276 (12) (1998) 1110-1116.

[81] K. Stana-Kleinschek, T. Kreze, V. Ribitsch, S. Strnad, Reactivity and electrokinetical properties of different types of regenerated cellulose fibres, Colloids Surf., A, 195 (1) (2001) 275-284.

[82] S.J. I'Anson, W.W. Sampson, S. Savani, Density dependent influence of grammage on tensile properties of handsheets, J. Pulp Pap. Sci., 34 (3) (2008) 182-189.

[83] S.J. I'Anson, W.W. Sampson, Competing Weibull and stress-transfer influences on the specific tensile strength of a bonded fibrous network, Compos. Sci. Technol., 67 (7) (2007) 1650-1658.